International Journal of Thermophysics, Vol. 25, No. 5, September 2004 (© 2004)

Interfacial Behavior in Type IV Systems[1]

A. Mejía[2, 3] and H. Segura[2]

Type IV mixtures exhibit two heteroazeotropic lines, one at low temperature and the other meeting the supercritical range, characterized by the proximity of their critical end points (CEPs). Between these CEPs, the liquid phase is homogeneous inside a narrow range of temperature. The aim of this work is to analyze interface properties and wetting transitions for Type IV mixtures. Interfacial tensions have been calculated by means of the gradient theory, applied to binary van der Waals fluids. This approach is able to predict interfacial tension and phase equilibrium using a common equation of state (EOS). Results show that interfacial properties and wetting conditions are governed by the densities and the number of phases involved in equilibrium, a scenario that changes as temperature evolves from the low- to the high-temperature heteroazeotropic line.

KEY WORDS: interface properties; square gradient theory; Type IV behavior; wetting transitions.

1. INTRODUCTION

Coexisting bulk fluid phases in thermodynamic equilibrium are connected by an interfacial fluid, whose concentration ρ, varies spatially between its bulk fluid phases. Fig. 1. shows, schematically, the typical pattern of ρ as a function of a spatial coordinate z, for a liquid in equilibrium with its vapor. For mixtures, the interfacial fluid may be enclosed by gas/liquid, liquid/liquid, or gas/liquid/liquid bulk fluids, and its $\rho(z)$ behavior is a function of pure fluids and their bulk densities. In fact, $\rho(z)$ may be or not be a monotonic function, as illustrated in Fig. 2.

[1] Paper presented at the Fifteenth Symposium on Thermophysical Properties, June 22–27, 2003, Boulder, Colorado, U.S.A.

[2] Department of Chemical Engineering, Group of Thermodynamics, Universidad de Concepción, POB 160-C, Concepción, Chile.

[3] To whom correspondence should be addressed. E-mail: amejia@diq.udec.cl.

0195-928X/04/0900-1395/0

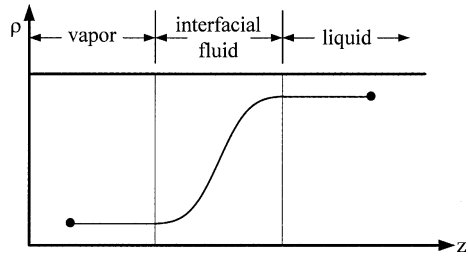

Fig. 1. Schematic representation of ρ–z projection for a planar vapor/liquid interface of a pure fluid at the boiling point. (•) VLE bulk densities.

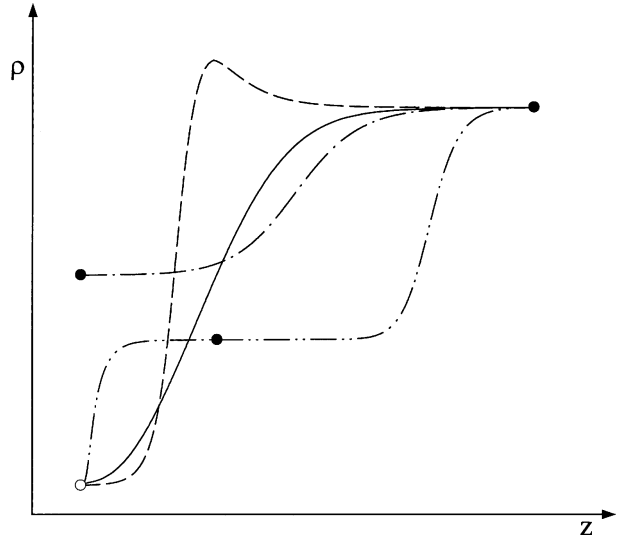

Fig. 2. Typical ρ_i–z projections for mixtures. (—) GL_1E, (– – –) GL_1E with adsorption of species on the interfacial zone, (–·–) L_1L_2E, (–···–) GL_1L_2E, (•) liquid bulk density, (○) vapor bulk density.

From a practical viewpoint, these kinds of interfaces are present in many chemical and environmental processes. For example, interface fluids are present in heat transfer under boiling conditions, generation of tropospheric ozone, liquid extraction processes, production of herbicides and pesticides, processes of enhanced oil recovery, fluids wetting, etc. Therefore, the analysis of interface fluid properties, such as interfacial tension and wetting transitions, are the precise piece to understand and design these industrial processes.

In this context, one of the most successful approaches is the square gradient theory of van der Waals [1]. Briefly, the gradient theory (GT) describes a continuous evolution of the density of the Helmholtz energy of an inhomogeneous fluid along the interface, from which the interfacial concentration profile and interface tension can be calculated. It should be noted that the main advantages of the GT approach are the facts that the interfacial behavior is described in the same terms as thermodynamic equilibrium variables, like temperature, pressure, and mole fraction, and that the same equation of state (EOS) model can be used to predict both the interfacial behavior and the phase equilibrium conditions. As follows from Rowlinson and Widom [1], the topology of an interface fluid is governed by the type of fluids and their phase equilibria; therefore, mixtures with several phase equilibrium patterns are adequate candidates to obtain a global understanding of interfacial behavior. Following the van Konynenburg and Scott work [2], Type IV mixtures are an interesting choice due to the fact these mixtures exhibit two heteroazeotropic lines (one at low and the other at high temperature) which are characterized by their critical end points (CEPs).

The main scope of this work is to analyze interface properties and wetting transitions for this kind of mixtures in a planar interface. Our predictions are based on GT applied to the van der Waals EOS (vdW-EOS) with a quadratic mixing rule (QMR). The results will be illustrated considering the behavior of the spatial variation of the fluid concentrations along the interface width and the dependence of the interfacial tension on equilibrium conditions.

2. THEORY

2.1. Square Gradient Theory for Planar Interfaces

GT was originally developed by van der Waals in 1894 and reformulated later by Cahn and Hilliard [3]. In this approach, the interfacial tension between two bulk phases (α,β) is related to the interface width by the following equation [1]:

$$\sigma = 2\int_{-\infty}^{\infty}\left(\Phi + P^0\right)dz = 2\int_{-\infty}^{\infty}\Delta\Phi\, dz \tag{1}$$

where σ is the interfacial tension, P^0 is the bulk equilibrium pressure, and z is a coordinate normal to the interface. The integral limits describe the boundary conditions of bulk fluid phases, i.e., $\rho_i(z=-\infty)=\rho_i^{\alpha}$ and $\rho_i(z=+\infty)=\rho_i^{\beta}$ where $\rho_i^{\alpha,\beta}$ corresponds to the molar concentration of

component i in the α and β bulk phases, respectively. Finally, Φ is the grand thermodynamic potential, which is defined as

$$\Phi[\rho_i, \rho] = a_0[\rho_i, \rho] - \sum_{i=1}^{n_c} \rho_i \mu_i^0 \left[T^0, V^0, \rho_i^0\right] \tag{2}$$

In Eq. (2) ρ is the concentration of the mixture which is related to the concentration of species i; ρ_i, and the mole fraction x_i by $\rho_i = x_i \rho$. n_c stands for the number of components. V^0, T^0, ρ_i^0 are the equilibrium volume, temperature, and concentration of component i, respectively. a_0 is the density of the Helmholtz energy of the homogeneous system ($a_0 = A/V$) and μ_i^0 is the chemical potential of component i at equilibrium. Both a_0 and μ_i^0 can be determined directly from any EOS. In Appendix A, we summarize these expressions for the vdW-EOS with QMR. An important feature of the Φ function, as stated by Rowlinson and Widom [1], is that the $\Delta\Phi$–ρ projection can be used to establish if the phase equilibria exhibit stable phases (absolute minima) or metastable phases (relative minima). An example of absolute and relative minima at $\Delta\Phi$–ρ projection can be observed in Fig. 3.

Replacing Eq. (2) in Eq. (1) reveals that the integration processes need an additional relation between ρ_i and z. Following the GT, this relation is given by the following set of partial differential equations (PDE) [4]:

$$\sum_{j=1}^{n_c} c_{ij} \frac{d^2\rho_j}{dz^2} - \frac{1}{2} \sum_{k,j=1}^{n_c} \frac{\partial c_{kj}}{\partial \rho_i} \frac{d\rho_k}{dz} \frac{d\rho_j}{dz} = \frac{\partial \Phi}{\partial \rho_i} \quad (i = 1, 2, \ldots, n_c) \tag{3}$$

where $\rho_i\big|_{z=-\infty} = \rho_i^\alpha$ and $\rho_i\big|_{z=\infty} = \rho_i^\beta$; c_{ij} is the cross influence parameter ($c_{ij} = c_{ji}$). Theoretically, c_{ij} is related to the mean square range of the direct correlation function of an homogeneous fluid. c_{ij} is given by [5]

$$c_{ij}(\rho, T) = \frac{\kappa T N_{av}^2}{6} \int_V s^2 c_0^{ij}(s; \rho)\, d^3 s \tag{4}$$

In this expression κ is Boltzmann's constant, N_{av} is Avogadro's number, s is a characteristic coordinate between species i and j, and $c_0^{ij}(s;\rho)$ is the two-body direct correlation function between species i and j in homogeneous fluids. However, since $c_0^{ij}(s;\rho)$ is intractable, some approximation has been applied [4]. One of the most successful approximations is $c_0^{ij}(s;\rho) \approx c_0^{ij}(s)$ [6], which automatically transforms the PDEs to a set of

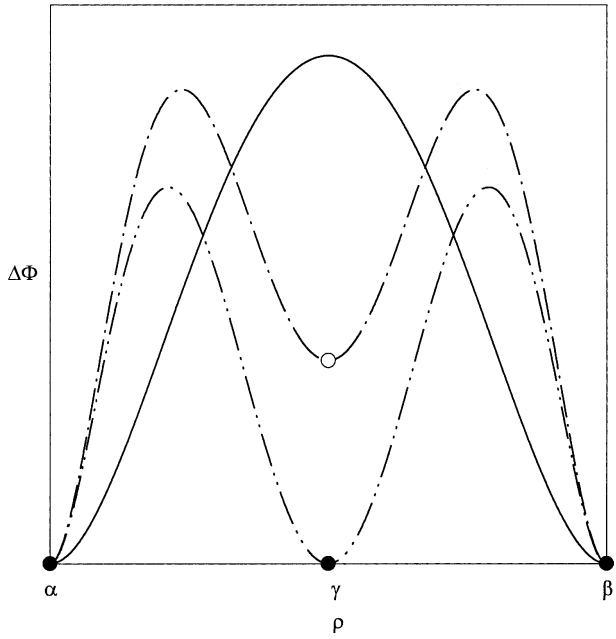

Fig. 3. Usual $\Delta\Phi$–ρ projections at fluid phase equilibria. (—) $\alpha\beta E$, (–·–) $\alpha\beta E$ with an embryo phase, γ, (–··–) $\alpha\beta\gamma E$, (•) absolute minima (stable phase bulk densities), (○) relative minima (metastable phases).

ordinary differential equations (ODEs). Based on c_0^{ij}'s approximation, c_{ij} for pure fluids ($c_{ij}=c_{ii}$) is given by [6]

$$c_{ii}(T)=-\frac{N_{\text{av}}^2}{6}\int_V s^2 u(s)g(s)d^3s \tag{5}$$

where u is the intermolecular potential and g is the radial distribution function. For the fluids studied here (vdW fluids), the Sutherland potential is used for u, and g is taken as a step function. u and g are given by

$$u_{ii}(s)=-\varepsilon_{ii}\left(\frac{\sigma_{ii}}{s}\right)^6, \quad g_{ii}(s)=\begin{cases}0 & \text{if } s<\sigma_{ii}\\ 1 & \text{if } s\geqslant\sigma_{ii}\end{cases} \tag{6}$$

ε_{ii} and σ_{ii} represent length and energy parameters characteristic of molecular interactions of specie i. Replacing Eq. (6) in Eq. (5) and integrating over V, c_{ii} takes the form,

$$c_{ii}=\frac{2}{3}N_{\text{av}}^2\pi\varepsilon_{ii}\sigma_{ii}^5 \tag{7}$$

Following Carey's work, Eq. (7) can be conveniently rewritten in terms of the cohesion parameter (a_{ii}) and the covolume (b_{ii}) as

$$\frac{c_{ii}}{a_{ii}b_{ii}^{2/3}} = \left(\frac{3}{2\pi N_{\text{av}}}\right)^{2/3} \tag{8}$$

For the vdW-EOS (see Appendix A), a_{ii} and b_{ii} are given by [7]

$$a_{ii} = \frac{27}{64}\frac{\left(RT_{\text{c},i}\right)^2}{P_{\text{c},i}} = \frac{2}{3}N_{\text{av}}^2\pi\varepsilon_{ii}\sigma_{ii}^3, \qquad \text{b}_{ii} = \frac{1}{8}\frac{RT_{\text{c},i}}{P_{\text{c},i}} = \frac{2}{3}N_{\text{av}}\pi\sigma_{ii}^3 \tag{9}$$

where R is the gas constant, and $P_{\text{c},i}$ and $T_{\text{c},i}$ are the critical pressure and the critical temperature for component i, respectively.

For the case of mixtures, c_{ij} can be obtained by averaging the pure-component influence parameters according to the following geometric combining rule [4]:

$$c_{ij} = \left(1 - \chi_{ij}\right)\sqrt{c_{ii}c_{jj}} \tag{10}$$

where χ_{ij} is a symmetric adjustable parameter ($\chi_{ij} = \chi_{ji}$) obtained by fitting experimental data of σ for mixtures. However, as some authors have shown [4,8], the use of $\chi_{ij} = 0$ is a good choice for several fluid/fluid interfaces. In the approximation presented here, all interfacial calculations were performed using $\chi_{ij} = 0$. The advantage of $\chi_{ij} = 0$ is that GT acquires a predictive character without a loss of generality [9,10], c_{ij} can be predicted from pure fluid information, and the ODEs simplify to the following system of algebraic equations (AEs) [4]:

$$\sqrt{c_{ss}}\left[\mu_k(\rho) - \mu_k^0\right] = \sqrt{c_{kk}}\left[\mu_s(\rho) - \mu_s^0\right] \quad k = 1, 2, \ldots, s-1, s+1, \ldots, n_{\text{c}} \tag{11}$$

These AEs can be solved by setting a value of $\rho_s(z)$ and calculating the ρ_k values. Once $\rho_k(\rho_s)$ have been determined, the $\rho_k(z)$ projections are calculated from the ODEs, which after some algebra yields [4,8]

$$z(\rho_n) - z_0(\rho_n^0) = \int_{\rho_n^0}^{\rho_n} \sqrt{\frac{1}{2\Delta\Phi}\sum_{i,j=1}^{n_{\text{c}}} c_{ij}\left(\frac{d\rho_i}{d\rho_n}\right)\left(\frac{d\rho_j}{d\rho_n}\right)}\,(d\rho_n) \quad n = 1, 2, \ldots, n_{\text{c}} \tag{12}$$

where z_0 is a reference of z coordinate, where $\rho = \rho_n^0$. Some patterns of $\rho_n(z)$ projections were shown for pure fluids and mixtures in Figs. 1 and

2, respectively. Eq. (12) also provides the possibility to express σ in terms of ρ rather than z. Replacing it in Eq. (1), $\sigma(\rho)$ is given by

$$\sigma = \int_{\rho_s^\alpha}^{\rho_s^\beta} \sqrt{2\Delta\Phi \sum_{i,j=1}^{n_c} c_{ij} \left(\frac{d\rho_i}{d\rho_s}\right)\left(\frac{d\rho_j}{d\rho_s}\right)}\, d\rho_s \tag{13}$$

The latter transformation is useful to understand the σ behavior near to critical states, and the wetting transition of interface fluids, as we will describe in the following section.

2.2. Numerical Procedure for Calculating Interfacial Properties

In order to calculate the interfacial behavior we have used the following procedure:

- Specify the critical temperature ($T_{c,i}$) and the critical pressure ($P_{c,i}$) for pure species i, and the interaction parameter (k_{ij}) of the mixture.
- At a given temperature T^0 and liquid phase mole fraction (x_i), perform the bubble-point calculation to predict the equilibrium pressure (P^0), the vapor-phase mole fractions (y_i) and the concentrations of the bulk phases ($\rho^{0,L}$, $\rho^{0,G}$). In this case, the vdW-EOS is used for predicting the equilibrium state and the ϕ–ϕ approach is considered for performing GLE calculations [7].
- Evaluate c_{ii} from Eq. (8) and c_{ij} from Eq. (10) with $\chi_{ij} = 0$.
- Select the independent variable ρ_s, provided that ρ_s must exhibit a monotonic behavior along the interface region. In this work, we selected $\rho_s = \rho_2$.
- Discretisize ρ_2 ($\rho_2 = \rho_s$) between the concentration of bulk phases ($\rho_2^{0,L}$ $\rho_2^{0,V}$). A discretization grid of 10,000 points has been considered in this work.
- Solve Eq. (11) for the concentration $\rho_{i\neq s}$ for each ρ_s value along the discretization grid. The Newton–Raphson method is used to solve Eq. (11) [11]. The derivatives involved in this numerical method can be calculated from

$$\left(\frac{d\rho_i}{d\rho_s}\right) = \frac{\sqrt{c_{ii}}\mu_{ss} - \sqrt{c_{ss}}\mu_{is}}{\sqrt{c_{ii}}\mu_{si} - \sqrt{c_{ss}}\mu_{ii}}, \quad \mu_{is} = \left(\frac{\partial \mu_i}{\partial \rho_s}\right)_{\rho_i, T, V} \tag{14}$$

- Calculate Φ from Eq. (2) and $\Delta\Phi$ as $\Delta\Phi = \Phi + P^0$.

- Evaluate $z(\rho_n)$ for $n=1,2$ from Eq. (12). The derivatives required in Eq. (12) have been calculated from Eq. (14) and the integration is performed considering an adaptive Gaussian Quadrature [11].
- Calculate σ from Eq. (13). The numerical integration procedure that allows calculation of σ is similar to the methods considered for integrating $z(\rho_n)$.

The previous procedure is summarized in Fig. 4.

2.3. Interfacial Tensions near Critical States

It is well known that when two phases (α, β) are approaching their critical state, the corresponding bulk phase densities become identical $(\rho^\alpha \approx \rho^\beta)$; therefore, Eq. (13) produces $\sigma \to 0$. For the case of three phases (α, β, γ), with $\rho^\alpha \neq \rho^\beta \neq \rho^\gamma$ along $\alpha\beta\gamma E$, interfacial tensions are different $(\sigma_{\alpha\beta} \neq \sigma_{\alpha\gamma} \neq \sigma_{\beta\gamma})$, but near to a CEP, $\rho^\alpha \neq \rho^\beta \approx \rho^\gamma$ which is conducive to $\sigma_{\alpha\beta} \approx \sigma_{\alpha\gamma}$ and $\sigma_{\beta\gamma} \to 0$.

2.4. Wetting Transitions at Fluid Interfaces

Considering Fig. 3 and following the structure of Eq. (13), we can conclude that the area below two bulk phases is proportional to σ, and, in general, when π different phases are in equilibrium, $[1/2(\pi-1)\pi]$ independent σs can be formed and are interrelated via their contact angles [1]. For the cases studied here, two (α,β) and three (α, β, γ) phases are in equilibrium; consequently, we have one $(\sigma_{\alpha\beta})$ or three $(\sigma_{\alpha\beta}, \sigma_{\alpha\gamma}, \sigma_{\beta\gamma})$ different interfacial tensions, respectively. In the later case, σs are interrelated by [1]

$$\sigma_{\alpha\beta} < \sigma_{\alpha\gamma} + \sigma_{\beta\gamma} \quad \text{Neumman inequality} \tag{15a}$$

$$\sigma_{\alpha\beta} = \sigma_{\alpha\gamma} + \sigma_{\beta\gamma} \quad \text{Antonow rule} \tag{15b}$$

and cyclic permutation of α, β, and γ. The situation described by Eq. (15a) is called partial wetting of the γ phase in $\alpha\beta$ interface. Equation (15b) denotes the total wetting of the γ phase in the $\alpha\beta$ interface, and the transition from partial to total wetting (or vice versa) is called the *wetting transition* [1], which can occur at a certain point along the three-phase equilibrium $(\alpha\beta\gamma E)$ line. The evolution of $\sigma_{\alpha\beta}$ along to $\alpha\beta\gamma$E is schematically illustrated in Fig. 5.

3. RESULTS AND DISCUSSION

Based on the global phase equilibria for the vdW-EOS [2], we select a typical Type IV mixture. Table I summarizes the critical properties of pure

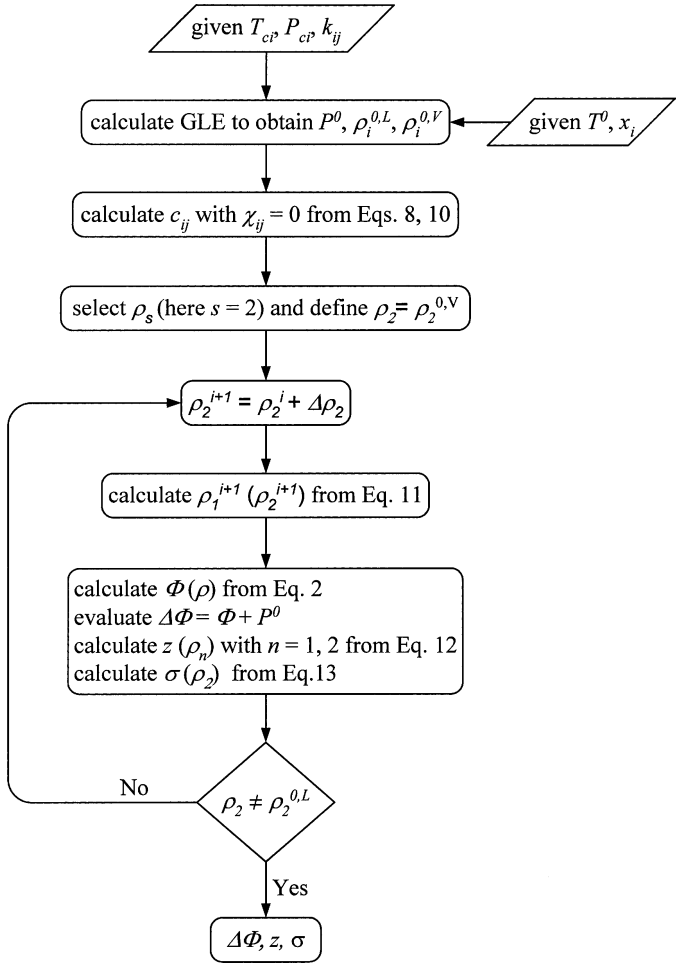

Fig. 4. Block diagram for algorithm calculations. T^0 is the isothermal condition to phase and interface calculations; $T_{c,i}$, $P_{c,i}$ are the critical temperature and the critical pressure for component i. k_{ij} is the interaction parameter. x_i is the liquid mole fraction of component i at phase equilibrium. P^0 is the bulk equilibrium pressure. $\rho_i^{0,L}$, $\rho_i^{0,V}$ are the bulk equilibrium concentrations of component i in liquid and vapor phases, respectively. c_{ij} are the influence parameters. ρ_i is the concentration of component i in the interface region. Φ is the grand thermodynamic potential. z is a coordinate normal to the interface. σ is the interfacial tension.

components and the interaction parameter for this mixture. Figure 6 illustrates its traditional pressure–temperature diagram, which exhibits three stable critical lines and two heteroazeotropic lines. The low temperature heteroazetropic line $[LLG]_1$ meets an upper critical end point $[UCEP]_1$,

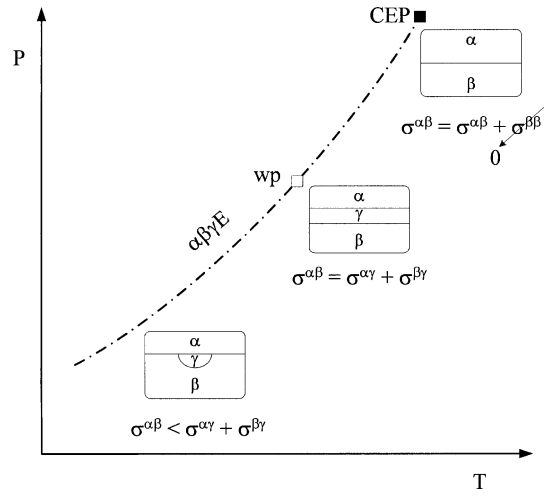

Fig. 5. Schematic representation of *wetting transition* along three-phase equilibria. α, β, γ phases. (–·–) Three phase equilibria ($\alpha\beta\gamma E$), (■) CEP, (□) wp (wetting point).

Table I. Critical Properties of Pure Components and Interaction Parameter

T_{c2}/T_{c1}	P_{c2}/P_{c1}	k_{12}
3.9692	6.1429	−0.3655

where the immiscible liquid phases of the heterazotrope become critical. At higher temperature, an additional heteroazeotropic line $[LLG]_2$ starts at a lower critical end point $[LCEP]_2$, where the liquid phase becomes immiscible again and, then, it ends at higher temperatures at $[UCEP]_2$, where one of the immiscible liquid phases and the gas phase of the heteroazeotrope become critical. Specific details related to Type IV and its construction can be found in Refs. [2,12]. In order to describe the interfacial behavior related to Fig. 6, we need to consider the topological evolution of interfacial projections (i.e., $\Delta\Phi$–$\rho, \rho_i, -z$ and σ–P, x_i) in the subcritical phase equilibria related to this type. Using the temperature as a variable, we are able to collect all subcritical equilibria in four zones. Table II summarizes these zones, their temperature ranges, and the isothermal conditions which will be used to analyze the interfacial behavior.

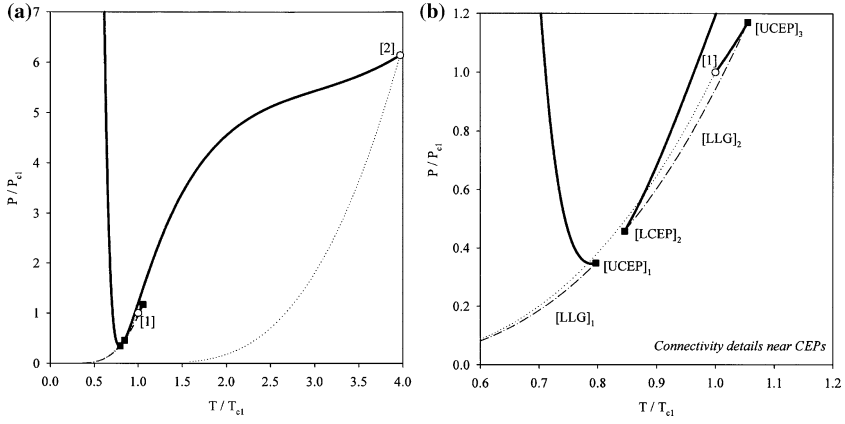

Fig. 6. Pressure – temperature diagram for Type IV mixtures. (—-) Critical line, (· · ·) vapor pressure, (–·–) GLLE, (○) pure component, (■) CEP.

Table II. Classification of Subcritical Phase Equilibria, and Isothermal Conditions for the Interfacial analysis

Zone	*Temperature Range* (T/T_{c1})	*Equilibria Type*	*Selected Temperature* (T/T_{c1})
1	0–0.7966 (T_{UCEP1})	GL_1, GL_2, L_1L_2	0.78
2	0.7966–0.8457 (T_{LCEP2})	GL	0.82
3	0.8457–1.0549 (T_{UCEP2})	GL_1, GL_2, L_1L_2	0.95
4	1.0549–3.9692 (T_{c2})	GL	1.10

In the following section we describe the interfacial topology in terms of the interfacial projections over the complete mole fraction range. We divide our analysis into two sections; one is related to the variation of the interfacial projections for each zone of a Type IV mixture (see Table II) and the other considers wetting transitions along the two heteroazeotropic lines.

3.1. Evolution of Interface Properties with Temperature

Figure 7 depicts the behavior of the $\Delta\Phi$–ρ profile at the four zones for the complete mole fraction range. From these figures, we can observe that each isothermal projection displays only two absolute minima for a fixed mole fraction. This fact confirms that two bulk fluid phases (GL or LL) are present at the temperature for which the fluid/fluid equilibria have been calculated, as we can expect from the theory and Table II. Additionally, Fig. 7 also shows some relative minima near to CEPs which are due

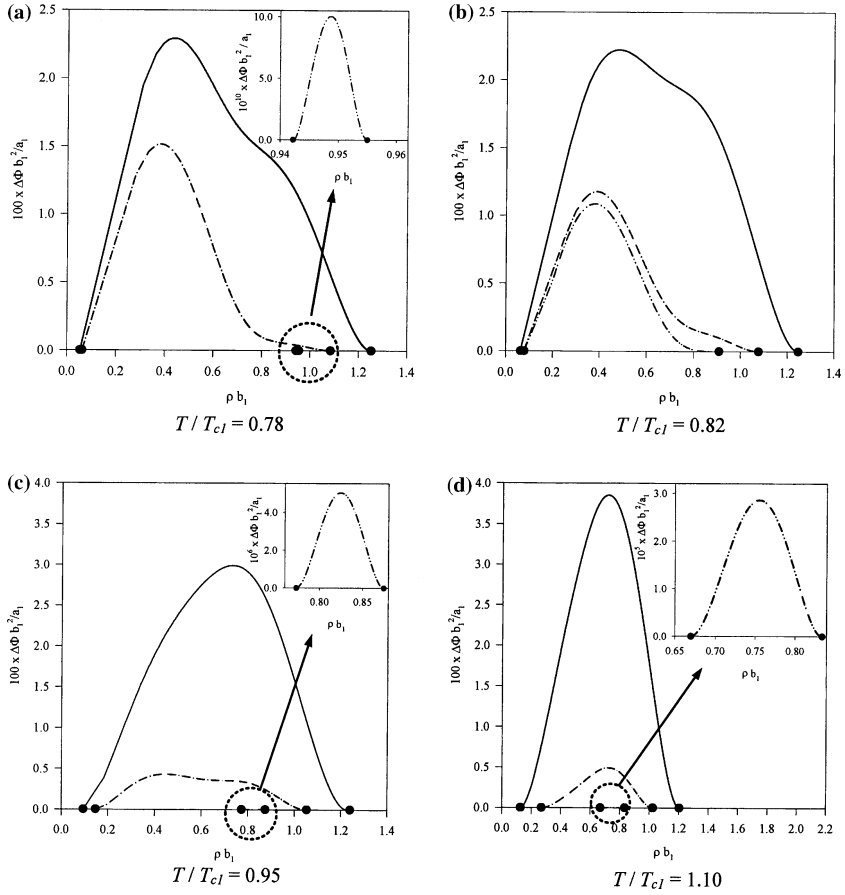

Fig. 7. $\Delta\Phi$–ρ projections at several isothermal conditions. (—) $x_1 = 0.25$, (– · –) $x_1 = 0.50$, (– · · –) $x_1 = 0.75$, (•) VLE bulk densities.

to the fact that an embryo phase (γ) is present. As is expected, the position and magnitude of γ changes as T or x_1 changes. For example, for an isothermal condition, γ changes from an embryo state to an equilibrium state (see Fig. 7(a) and (c)) as x_1 increases. At a fixed x_1, the density of γ may change from liquid-like to gas-like densities as T increases. In addition, from the theoretical arguments, we can anticipate, from $\Delta\Phi$–ρ diagrams, that σ_{GL} is not always greater than σ_{LL}. The σ value depends on the thermomechanical conditions at which the equilibrium is calculated.

Figure 8 illustrates the concentration of species along the interface length. These ρ_i–z projections were calculated at the same thermodynamic

conditions as Fig. 7. Inspection of these diagrams reveals that the more volatile component (1) always shows a stationary point (SP), when its concentration is larger than the bulk concentration. This fact reflects that component (1) is positively adsorbed at the interface. Moreover, the less volatile component (2) is not adsorbed. From these figures we can observe that the position and magnitude of SPs change as T or x_1 changes. In fact, we can conclude that both the position and magnitude of SPs increase as x_1 increases. For a fixed x_1, the position of SP increases and the magnitude decreases as T increases. Figure 8 also shows that LL interfaces exhibit smoother profiles and larger interface widths than GL

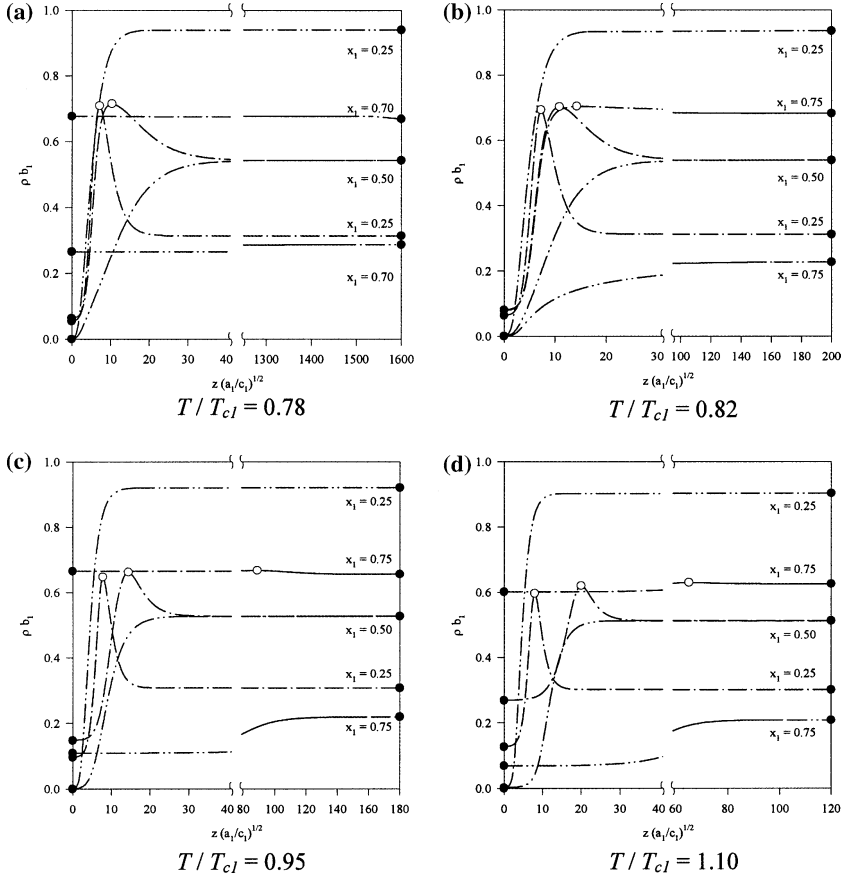

Fig. 8. ρ_i–z projections at several isothermal conditions. (–·–) ρ_1, (–···–) ρ_2, (•) VLE bulk densities, (○) stationary points (sps).

interfaces. This behavior is caused, mainly, by the bulk concentration gradient in LLE and in GLE. Finally, when previous patterns are compared with computer simulations [13], we can conclude that ρ_i–z from GT, shows good qualitative agreement to simulations for LL and GL interfaces.

Figure 9 shows the σ–P projections at the same isothermal conditions considered in Figs. 7 and 8. As expected from Table II, one or three interfacial tensions (σ_{GL} or σ_{GL1}, σ_{L1L2}, σ_{GL2}) are present in these $\sigma(P)$ diagrams. A quick inspection of each isothermal σ–P diagram reveals that,

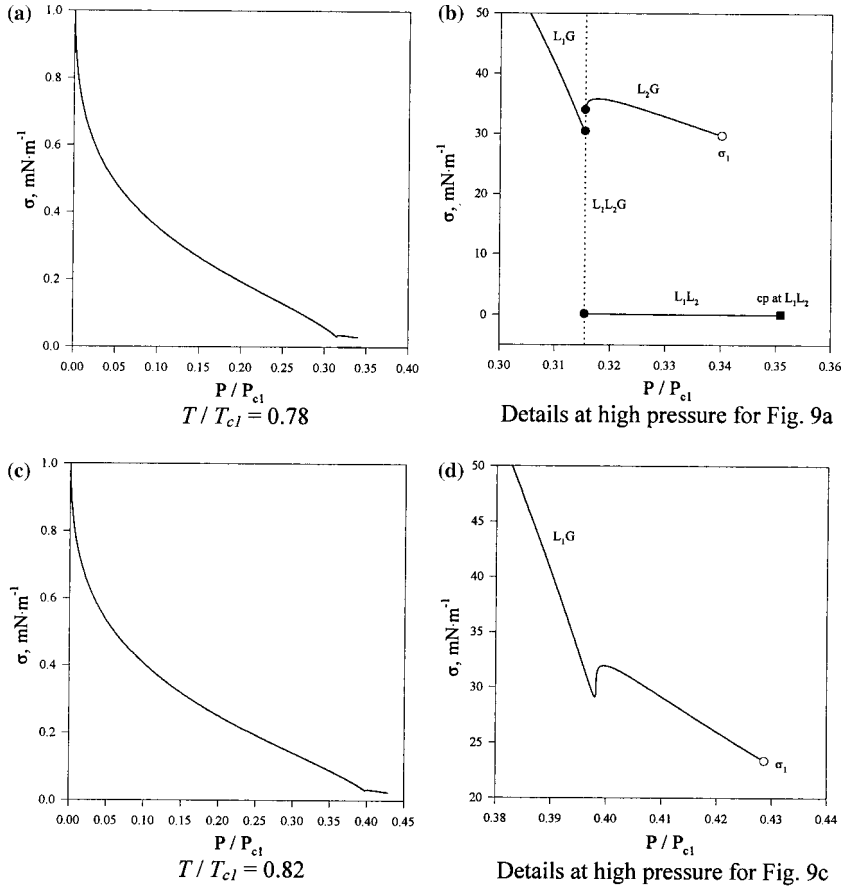

Fig. 9. σ–P diagrams at several isothermal conditions. (· · ·) L_1L_2GE, (•) three-phase line, (○) pure component, (■) cp (critical point).

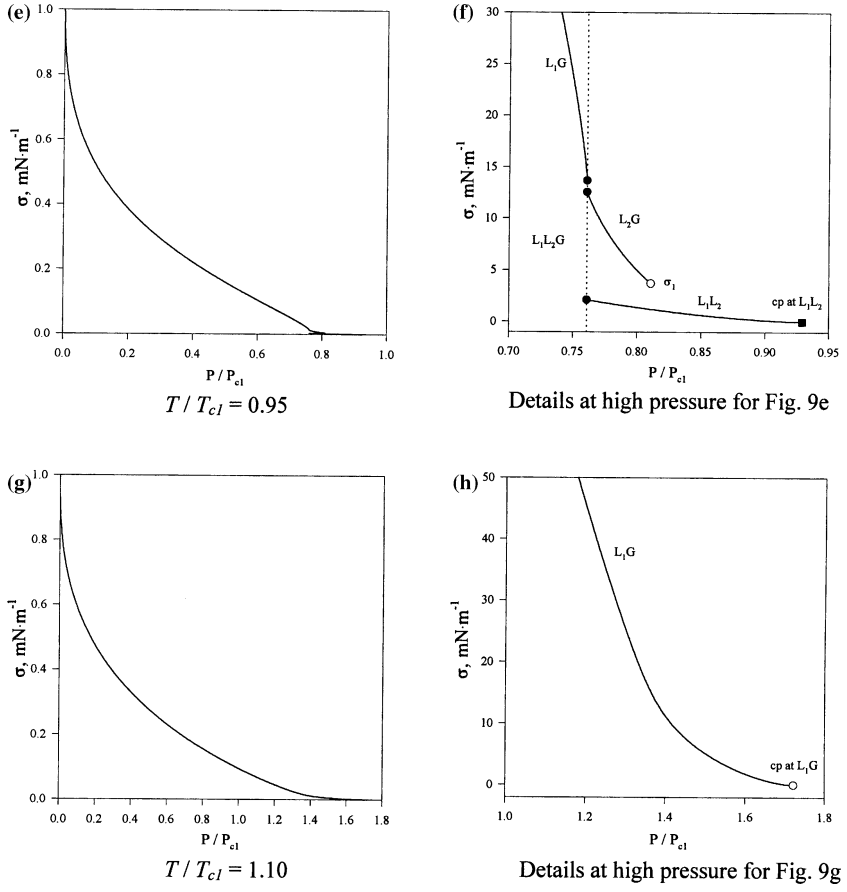

Fig. 9. Continued.

in general, σ decreases as the phase equilibrium tends to the critical point, as expected from Eq. (13). However, a close inspection shows that σ may increase in regions where the γ phase is present. The $\sigma(P)$ behavior can be summarized as follows: σ is not a continuous function in zones 1 and 3, its discontinuity is due to the fact that three equilibria conditions are present into these zones (see Table II). In particular, zone 1 shows that $\sigma_{GL1}, \sigma_{GL2} > \sigma_{L1L2}$. Zone 3 shows two regimes as the temperature increases; from T_{LCEP2}/T_{c1} to $T/T_{c1} = 1$, $\sigma(P)$ is similar to zone 1, and from $T/T_{c1} = 1$ to T_{UCEP2}/T_{c1}, $\sigma_{GL1} > \sigma_{L1L2} > \sigma_{GL2}$. For zones 2 and 4, σ is a continuous function of P; however, its trend is affected by the presence of the γ phase. In order to complete the σ descriptions in zones 1–4,

Fig. 10 shows the evolution of the interfacial tension on mole fraction $\sigma(x_1)$. From these figures we can observe similar patterns discussed previously. Regrettably, no experimental information is available to contrast our $\sigma(P, x)$ predictions. However, we can observe that our description reflects the facts in their phase diagrams, and follows the same patterns observed by other authors [8].

3.2. Wetting Transitions along to Three-Phase Equilibria

Figure 11 shows σ–T projections along the two three-phase equilibria for the Type IV mixture, and Table III summarizes its behavior as temperature increases. From Table III, we can establish that at a CEP three-phase

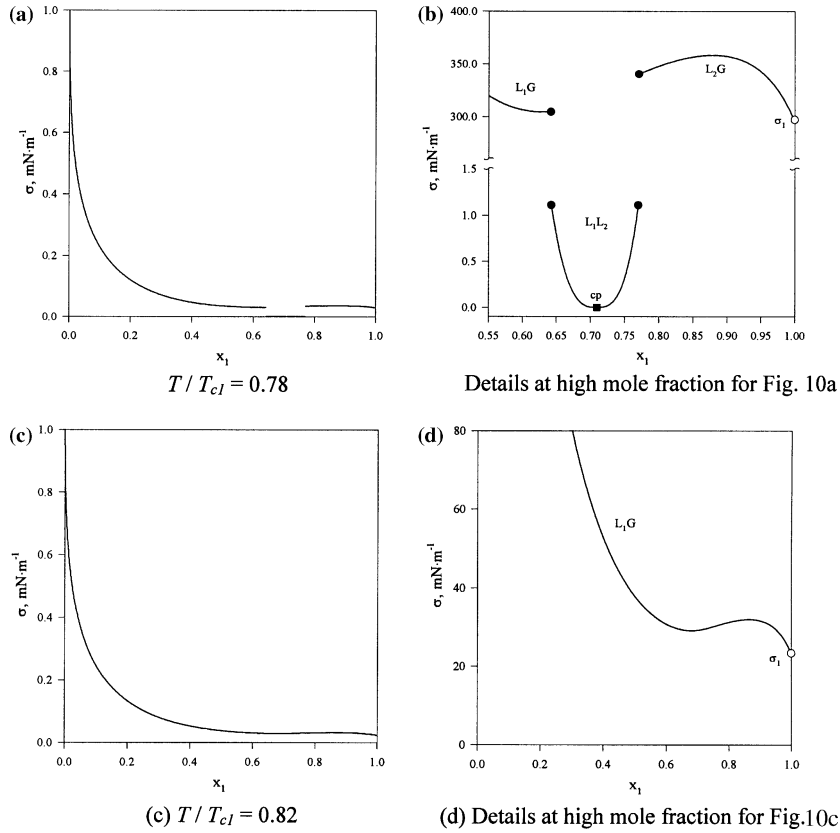

Fig. 10. σ–x_1 diagrams at several isothermal conditions. (•) Three-phase line, (○) pure component, (■) cp (critical point).

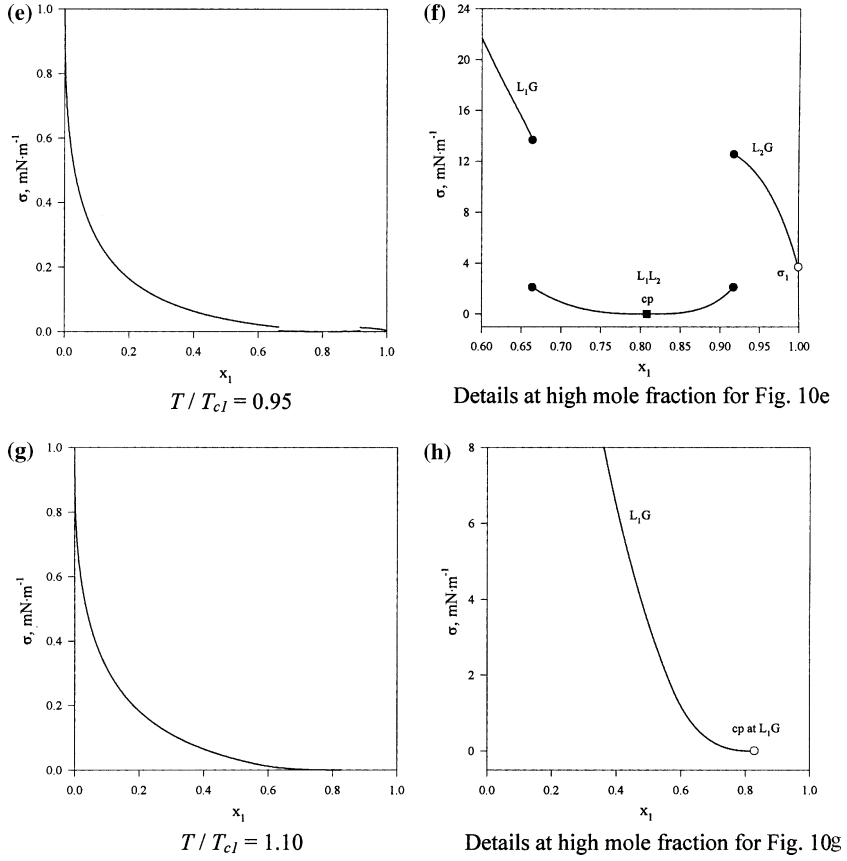

Fig. 10. Continued.

equilibria converge, simultaneously, to one subcritical equilibria and one critical equilibria. These interfacial tension results agree with the phase description from van Konynenburg and Scott. In addition, from these figures and Eqs. (15), we can conclude that along the $[GLL]_1$ line, wetting transitions never occur. But along $[GLL]_2$, $\sigma_{GL2} = \sigma_{GL1} + \sigma_{L2L1}$ at $T/T_{c1} = T_w/T_{c1} = 0.9153$, and therefore, the $[GLL]_2$ line exhibits a wetting transition. Physically, this transition means that for the GL_2 interface, a layer of a second liquid phase (L_1) intrudes between G and L_2 phases. In complement, it is important to state that $\rho_i(z)$ and $\Delta\Phi(\rho)$ show the expected behavior of a three-phase equilibrium (see Figs. 2 and 3). These behaviors reinforce the phase and interface patterns previously described.

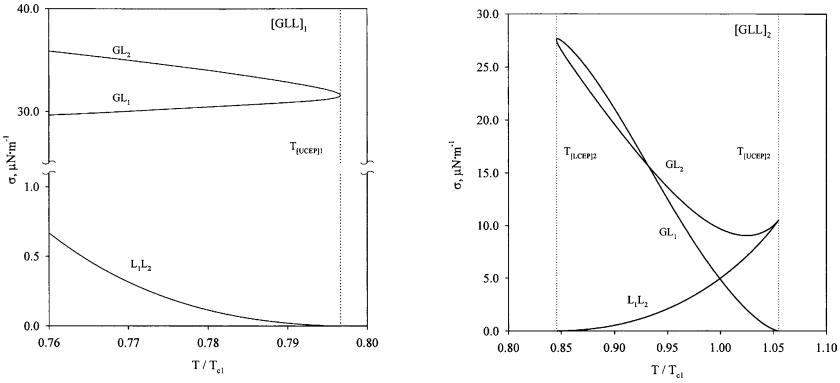

Fig. 11. σ–T diagrams along $[GLL]_1$ and $[GLL]_2$.

Table III. Interfacial Tension Behavior along Three-Phase Equilibria for Type IV Mixture

Temperature range	Phase equilibria type	Interfacial tension behavior
$[GLL]_1$ line		
Subcritical equilibria		
$T < T_{UCEP1}$	GL_1, L_1L_2	σ decreases as T increases
	GL_2	σ increases as T increases
Subcritical equilibria		
$T = T_{UCEP1}$	$GL_1 = GL_2$	$\sigma_{GL1} = \sigma_{GL2} \neq 0$
Critical equilibria		
	L_1L_2	$\sigma_{L1L2} = 0$
$[GLL]_2$ line		
Subcritical equilibria		
$T = T_{LCEP2}$	$GL_1 = GL_2$	$\sigma_{GL1} = \sigma_{GL2} \neq 0$
Critical equilibria		
	L_1L_2	$\sigma_{L1L2} = 0$
Subcritical equilibria		
$T_{LCEP2} < T < T_{UCEP2}$	GL_1, GL_2, L_1L_2	σ_{GL1} first decreases and then increases, σ_{L1L2} decreases and σ_{GL2} increases as T increases
Subcritical equilibria		
$T = T_{UCEP2}$	$GL_1 = L_1L_2$	$\sigma_{GL1} = \sigma_{L1L2} \neq 0$
Critical equilibria		
	GL_2E	$\sigma_{GL2} = 0$

4. CONCLUDING REMARKS

In this work we analyze interfacial properties and wetting transitions for Type IV mixtures using the GT and the vdW-EOS with QMR. The advantage of this approach is that a common EOS can be used to predict phase equilibrium as well as interfacial properties. This advantage brings the possibility to explain the phase equilibria and its stability from the interfacial behavior. According to results, interfacial properties and wetting conditions are governed by the densities and the number of phases involved in equilibrium, a scenario that changes as temperature evolves from the low- to the high-temperature heteroazeotropic line.

ACKNOWLEDGMENT

This work was financed by FONDECYT, Santiago, Chile (Project 2010100).

APPENDIX A: Density of the Helmholtz energy of the homogeneous system (a_0) and chemical potential of component i (μ_i^0) from van der Waals equation of state.

The van der Waals equation of state (vdw-EOS) is given, in terms to $P(T, \rho)$, by

$$P = \frac{RT\rho}{1-\rho b} - a\rho^2 \tag{A.1}$$

where P is the absolute pressure, T is the absolute temperature, R is the gas constant, ρ is the concentration of the mixture, a is the cohesion parameter of the mixture, and b is the covolume of the mixture. Using the QMR, a and b are given by

$$\rho^2 a = \sum_{\mathrm{i,j}=1}^{n_c} \left(1-k_{ij}\right) \rho_i \rho_j \sqrt{a_{ii} a_{jj}}, \quad \rho b = \sum_{i=1}^{n_c} \rho_i b_{ii} \tag{A.2}$$

where n_c stands for the number of components, ρ_i is the concentration of species i, a_{ii}, and b_{ii} are the cohesion parameter, and covolume of species i, respectively (see Eq. (9)). k_{ij} is the interaction parameter.

a_0 and μ_i^0 can be calculated by used the following relations [7,14]:

$$\frac{a_0}{\rho RT} = \int_0^{\rho} \left(\frac{P}{RT\rho^2} - \frac{1}{\rho}\right) d\rho + \frac{1}{\rho} \sum_{i=1}^{n_c} \rho_i \ln \rho_i, \quad \mu_i^0 = \left(\frac{\partial a_0}{\partial \rho_i}\right)_{\mathrm{T},\rho_j} \tag{A.3}$$

For the case of the vdW-EOS applied to a multicomponent fluid, Eq. (A.3) can be expressed as

$$a_0 = -a\rho^2 - RT\rho \ln(1-b\rho) - RT \sum_{i=1}^{n_c} \rho_i \ln\left(\frac{P_{\text{ref}}}{RT\rho_i}\right) \tag{A.4}$$

$$\mu_i^0 = -RT \ln(1-b\rho) + \frac{b_i RT\rho}{(1-b\rho)} - 2\sum_{j=1}^{n_c} a_{ij}\rho_j - RT \ln\left(\frac{P_{\text{ref}}}{RT\rho_i}\right) + RT \tag{A.5}$$

where P^{ref} is some freely chosen reference pressure.

REFERENCES

1. J. S. Rowlinson and B. Widom, *Molecular Theory of Capillarity* (Oxford University Press, Oxford, 1982).
2. P. van Konynenburg and R. Scott, *Phil. Trans. R. Soc. (London)* **298A**:495 (1980).
3. J. W. Cahn and J. E. Hilliard, *J. Chem. Phys.* **28**:258 (1958).
4. B. S. Carey, *The GradientTheory of Fluid Interfaces,* Ph.D. Thesis (University of Minnesota, 1979).
5. V. Bongiorno, L. E. Scriven, and H. T. Davis, *J. Colloid Interf. Sci.* **57**:462 (1976).
6. B. F. McCoy and H. T. Davis, *Phys. Rev. A* **20**:1201 (1979).
7. H. Van Ness and M. Abbott, *Classical Thermodynamics of Nonelectrolyte Solutions* (McGraw-Hill, New York, 1982).
8. P. M. W. Cornelisse, *The Gradient Theory Applied, Simultaneous Modelling of Interfacial Tension and Phase Behaviour* , Ph.D. Thesis (Delft University, 1997).
9. D. E. Sullivan, *J. Chem. Phys*. **77**:2632 (1982).
10. M. E.Costas, C. Vera, and A. Robledo, *Phys. Rev. Lett*. **51**:2394 (1983).
11. R. G. Rice and D. D. Do, *Applied Mathematics and Modeling for Chemical Engineers* (Wiley, New York, 1995).
12. J. S. Rowlinson and F. Swinton, *Liquids and Liquid Mixtures* (Butterworths, London, 1982).
13. J. Winkelmann, *J. Phys.: Condens. Matter* **13**:4739 (2001).
14. J. Wisniak, A. Apelblat, and H. Segura, *Chem. Eng. Sci.* **53**:743 (1998).